Acta Acustica united with Acustica
Vol. 104 (2018) 685 – 696

Technical and Applied Papers
DOI 10.3813/AAA.919208

Numerical Simulation of Sound Propagation through the Can-Annular Combustor Exit

Federica Farisco[1)], Lukasz Panek[1)], Jim B. W. Kok[2)]
[1)] Power Generation Division - Gas Turbines, Siemens AG - Section Energy, Huttenstrasse 12, 10553 Berlin, Germany. federica.farisco@gmail.com
[2)] University of Twente, ET/Thermal Engineering, Drienerlolaan 5, 7522 NB, Enschede, The Netherlands

Summary
Thermo-acoustic instabilities in high power density gas turbine engines have to be predicted in order to avoid unexpected shutdown events. To predict these instabilities, the acoustics behavior of the combustion system needs to be analyzed. The work presented in this paper on combustor-turbine interaction is focused on reflection coefficient analysis. The study is based on a simplified two-dimensional (2D) geometry representing the vane section and another geometry corresponding to a real engine alike combustor/turbine design. Compressible Large Eddy Simulation (LES) is applied based on the open source Computational Fluid Dynamics package OpenFOAM. A forced response approach is used imposing a sound wave excitation at the inlet of the combustion chamber. The applied Non-Reflecting Boundary Conditions (NRBC) are verified for correct behavior and plausibility of the acoustic set up. Multi-harmonic excitation with small amplitudes is used to preserve linearity. The numerical results are compared to analytical formulae in order to test the validity of both approaches for the chosen geometries.

PACS no. 43.20.-f, 43.28.-g

1. Introduction

Thermo-acoustic instabilities in gas turbines limit the operational range and represent an issue that needs to be studied, especially in lean premixed combustion technology. The correct modelling of acoustic oscillations in combustors requires a detailed knowledge of the boundary regions directly influencing the phenomena leading to instability. The analysis of the reflection coefficient of the combustor and turbine interface is the focus area of this study. In this work a numerical investigation of the acoustic behavior of two related geometries with a different level of complexity is performed. The engine configuration to which this study is related is presented in Figure 1.

It is a can-annular stationary gas turbine. Clearly the multiple combustor cans can be seen. The exit passages of all cans together feed the turbine inlet over the circumference. In the numerical studies presented, the sound waves originating from thermo-acoustic instabilities in the real system are replaced by artificial ones using a forced response approach. An excitation has been applied at the inlet, and the resulting acoustic perturbations traveling upstream and downstream of the turbine stator stage were analyzed.

The current publication focuses on the acoustic perturbations excluding entropy waves. It analyzes the reflection coefficient for a simplified 2D geometry in comparison to the results obtained for a complex geometry 3D model. The numerical data is compared to analytical solutions for quiescent and subsonic flow conditions. The innovation of this work consists of the extraction of data from numerical simulations (LES) of a realistic 3D case including the downstream section of a combustion can and the first turbine vane row.

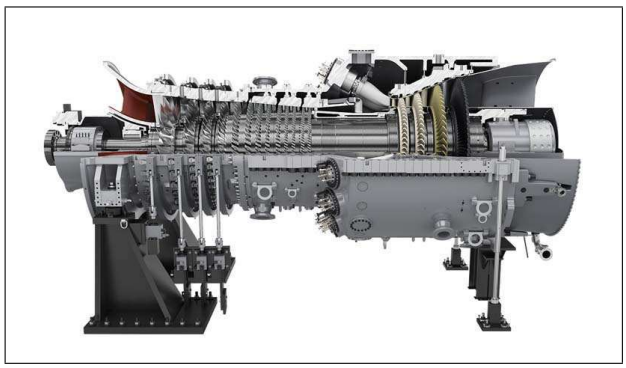

Figure 1. Model of a can-annular gas turbine, see https://www.siemens.com/global/en/home/products/energy/power-generation/gas-turbines/sgt6-8000h.html/

The reflection and transmission of sound, vortices and entropy perturbation through passages between turbine blades or vanes has been studied in depth the past four decades. The investigations were focused on the explanation of the so called excess noise [1, 2, 3] with the entropy

Received 12 July 2017,
accepted 19 May 2018.

fluctuations in the foreground, but also resulted in valuable formulations for the remaining solution modes. They show how direct and indirect combustion noise sources need to be taken into account and present predictions based on analytical models and empirical data. The direct combustion noise mechanism concerns the generation by the turbulent flame of heat release perturbations, that lead to the propagation of acoustic perturbations upstream in the combustor or downstream through the turbine stages. The indirect noise refers to the noise generated when entropy fluctuations are accelerated passing through the turbine stages. The flames are then just indirectly involved in the noise generation.

Different kinds of analytical models have been used in order to study the propagation of acoustic, entropy and vortical waves. Leyko *et al.* [4] present the results for a simplified one-dimensional (1D) model combustor with the calculated indirect combustion noise to be 10 times larger than the direct noise. In the work of Marble [2] and Marble and Candel [3] the interaction of entropy and pressure waves in choked and not choked nozzles is studied and treated in one dimension.

Crocco [5] and Tsien [6] study also the generation of acoustic waves in case of 1D nozzles. Bake *et al.* [7] analyze experimentally through the entropy wave generator (EWG) the indirect noise for a 1D nozzle. Review papers by Lamarque and Poinsot [8], Mühlbauer et al. [9], Leyko *et al.* [10] and Duran *et al.* [11] provide an overview of the experimental and numerical studies related to the reflection coefficient analysis. They represent inlets and outlets of chambers as one-dimensional ducts and evaluate impedances of subsonic and supersonic choked nozzles through analytical formulae and numerical methods using Linearized Euler Equations (LEE). They show how the theory of the 1D compact nozzle of Marble nd Candel [3] works for these configurations. Furthermore the work of Leyko *et al.* [12] demonstrates the use of analytical models for 1D and 2D flows and the usage of the compact noise assumption for 1D models.

Cumpsty and Marble [13] treat a system related closer to a gas turbine situation where perturbations are interacting with a turbine blade row. They study wave transmission and generation including entropy waves through an axially compact blade row in a 2D periodic and inviscid flow. Muir [14, 15] studies an infinitely thin blade row instead of a 2D geometry using the actuator-disk theory. Kaji [16, 17] has shown a semi-actuator disk theory taking into account infinitely thin spacing between the blades and finite chord-length, and he has analyzed a method focused on the acceleration potential to study the sound transmission through a 2D rectilinear cascade. Many models in 1D and 2D have been applied but only few real three-dimensional (3D) cases have been studied until now.

An example is given by Posson [18, 19] that shows results on a 3D rectilinear cascade model for entropy noise generation that takes into account cascade effects and finite chord neglecting the angle of deviation. The current study investigates the analytical model of Cumpsty and Marble [13] verifying and comparing it with the numerical results obtained for the 2D configuration focusing on the propagation of acoustic waves. The numerical analysis performed for the 2D geometry is compared also with the numerical results obtained for the 3D configuration. This last part, related to the analysis and comparisons studied between the 2D and 3D systems, distinguishes this work from the previous papers cited.

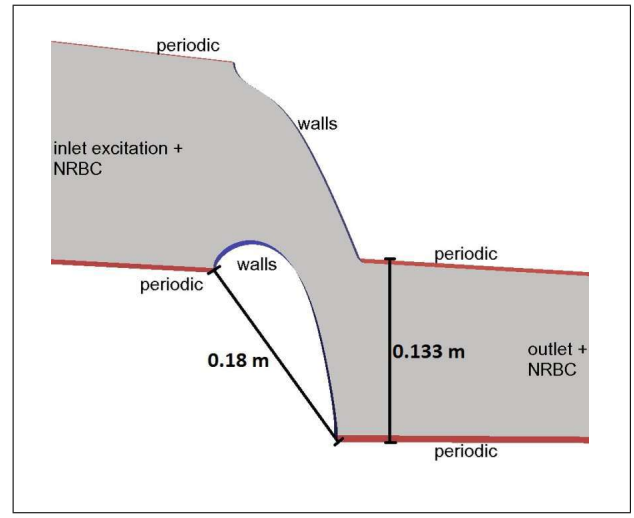

Figure 2. Overview of the 2D single vane geometry investigated with periodicity.

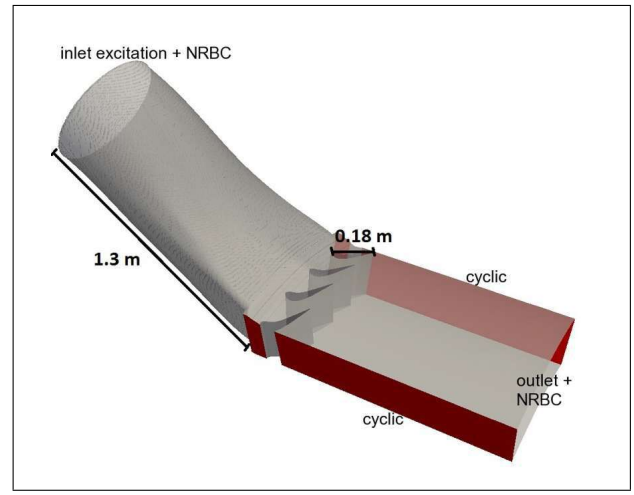

Figure 3. 3D can and stator stage with artificial extensions upstream and downstream.

2. Investigated Configurations

The cases selected for the analysis are shown in Figure 2 and Figure 3 and described below in more detail. These configurations have been chosen because they represent typical elements found in modern gas turbines.

The studied geometries have been considered as a simplification of technical configurations as a first step to the real engine analysis. The 2D stator vane passage (Figure 2) represents well a realistic stator stage if no gra-

dients are assumed along the airfoil span. The limitation to 2D reduces the computational time significantly. This setup presents a good trade-off between accuracy and numerical effort. Due to periodicity, the passage has equal cross-sections before and after the profile. The 3D geometry (Figure 3) is a representation of a can-annular system often found in modern gas turbines. Since the 2D geometry is built with the same airfoil and equivalent cross-section, it is expected to obtain similar results for equal flow conditions. In terms of acoustic behavior it should be similar to the 2D single vane previously described.

3. Numerical Method

3.1. LES Compressible Solver

For all simulations compressible LES has been applied based on the open source CFD code OpenFOAM. A compressible solver (sonicFoam) with up to second order discretization in space and time has been used to compute the solutions. At first, the LES One Equation Eddy Viscosity Model for compressible flows has been used. The Eddy viscosity sub-grid scale (SGS) model is based on a modeled balance equation to simulate the behaviour of the kinetic energy k. The applied relations are presented in Equations (1) and (2),

$$\frac{\mathrm{d}}{\mathrm{d}t}\rho k + \mathrm{div}\rho U k - \mathrm{div}\mu_{\mathrm{eff}}\nabla k = -\rho D : B - \frac{c_e \rho k^{\frac{3}{2}}}{\Delta} \tag{1}$$

and

$$B = \frac{2}{3}k I - 2\nu_{\mathrm{sgs}}\,\mathrm{dev}D, \tag{2}$$

where $D = \mathrm{symm}\nabla U$ with "symm" that denotes the symmetric part of the tensor, $\mathrm{dev}D$ indicates the deviatoric part of the tensor, kinematic viscosity $\nu_{\mathrm{sgs}} = c_k\sqrt{k}\Delta$ with Δ as filter width, effective viscosity $\mu_{\mathrm{eff}} = \mu_{\mathrm{sgs}} + \mu$ with μ_{sgs} as turbulence eddy viscosity caused by the Reynolds stresses and μ as dynamic viscosity, model coefficients $c_e = 1.048$ and $c_k = 0.094$. The calculated turbulent Reynolds number at the vane chord exit had a value of $\Re e \approx 2 * 10^6$.

In parallel it has been decided to run also simulations with laminar flow, since the main aspect of the work is related to the acoustic behavior of the systems. No turbulence was modeled when applying the simplication of the laminar flow. Turbulence or boundary layers have not been taken into account in these last simulations to isolate the noise generation due to the force response approach from other possible sources. In this last numerical implementation the dynamic viscosity was fixed as a property inherent to the fluid and the turbulence eddy viscosity caused by the Reynolds stresses was assumed to be equal to zero. These simulations were done just for a first fast results check. LES has been applied to analyze the results with much higher accuracy. The results shown in this paper have been obtained from the LES simulations with subgrid turbulence model.

For the 3D case a Courant number of $Co < 1$ has been maintained with time step $\Delta t = 1e-06$ s running the simulation for about 200 ms real time.

3.2. NRBC and Periodicity

Non-Reflecting Boundary Conditions (NRBC) have been used at the inlet and outlet of the geometries. The role of the NRBC is to impose the flow conditions while suppressing acoustic wave reflections.

The NRBC applied damps the longitudinal modes. The current analysis focuses on longitudinal modes. A more detailed modal analysis would need to be performed in order to study the presence of radial and circumferential modes. The derivation of the NRBC is based on Local One-Dimensional Inviscid (LODI) relations to obtain approximate values for the wave-amplitude variations in terms of the primitive flow variables as shown in [20], [21], [22] and [23]. A relaxation factor has been introduced for the wave coming from outside of the domain, with the aim to define fixed mean pressure at the outlet or fixed mean velocity at the inlet.

This factor is related to the time scale τ that must be as small as possible to avoid large deviations of the boundary conditions from the determined mean value. On the other hand, for small time scales the boundary conditions become fully reflective. Therefore there is the need to find a compromise between reflection and allowed pressure drift. This fact led to the choice of $\tau = 0.01$ s for all simulations and NRBCs of this study. For the cases analyzed, the periodicity has been taken into account. Figure 2 and Figure 3 show the boundary conditions applied for both 2D and 3D configurations in detail. The periodic patches were conforming and no interpolation was necessary. The walls of the can have been set as rigid. The viscosity has been not taken into account since the main focus of the study was related to acoustics.

3.3. Flow

Each geometry has been investigated using different mass flows $\dot{m}$ at the inlet resulting in different Mach numbers. The values of temperature $T_{\mathrm{in}} = 1700$ K set at the inlet and pressure $p_{\mathrm{out}} = 1050000$ Pa at the outlet have been applied for the different configurations. The operating conditions have been varied maintaining non-choked flow in the throat ($M < 1$) of the vane section. In the following only the case without flow for the 2D geometry and with a Mach number in the throat $M \approx 0.7$ for both 2D and 3D configurations are presented.

3.4. Meshing

The computational mesh of the 2D case analyzed consists of about 70000 cells. The mesh has been generated through the tool blockMesh with one cell in depth. Additional wall refinements have been used around the vanes in order to resolve the flow with more accuracy in this section.

A cell stretch with a factor of 3 has been applied in the outlet area for an increased dissipation of flow structures hitting the outlet boundary. The mesh for the 3D engine case consists of about 3 Million cells and the mesh has also been generated using the tool blockMesh but additionally using the tool snappyHexMesh to mesh the complicated boundary surface. The quality of the CFD results has been evaluated focusing on the main parameters obtained in the numerical simulations comparing them with the values of pressure, temperature, Mach number, velocity listed in tables proven by the experiments and past validations done at Siemens. The numerical results have been compared with flow parameters and data available at Siemens. After demonstration of the match between the flow parameters available and the numerics, comparisons between the current numerical results and analytical data have been performed. No comparisons with experiments with flow have been taken into account in this study.

3.5. Forced Response Approach

A forced response approach has been used during the simulations, imposing a velocity-based wave excitation at the inlet of the combustion chamber. The signal applied is a superposition of multiple sine signals with a randomized phase. frequency range of $f = 20-2000\,\mathrm{Hz}$, has been used at small amplitudes of less than 1% of the mean values to stay in the linear regime. The forcing applied is longitudinal without including any circumferential modes. Pressure and velocity signals have been recorded at various points along the flow path during the numerical calculations. The post-processing for all cases is performed using the multi-microphone method in order to calculate the reflection coefficient, taking into account the effects of the mean flow. This method will be discussed in detail in Section 3.6.

3.6. Multi-Microphone Method

The multi-microphone method can be considered as an extension of the two microphone method and it has been described by several authors. The method presented in this work refers to the works of Schuermans [24], Polifke *et al.* [25] and Paschereit *et al.* [26, 27]. The Riemann invariante $\hat{p}^+$ and $\hat{p}^-$ are considered as the forward and backward traveling waves and their complex amplitudes $\hat{p}(x_m)$ are derived from the measured values of three (or more) microphones. Multiple axial pressure measurements are used in the current method in order to obtain an accurate approximation to the Riemann invariants in the frequency domain. In this case, the system of equations is overestimated because the number of equations (3 or more) is larger than the number of unknowns (2) and cannot be solved by the application of conventional methods.

From the one-dimensional wave equation, the plane wave acoustic field is decomposed into the upstream and downstream propagating part $\hat{p}^+$ and $\hat{p}^-$. Each microphone amplitude is composed of traveling waves $\hat{p}^\pm$ by

$$\hat{p}(x_m) = \hat{p}^+ \mathrm{e}^{-\mathrm{i}k^+x_m} + \hat{p}^- \mathrm{e}^{\mathrm{i}k^-x_m}, \tag{3}$$

where $k^\pm = \omega/(c \pm \overline{u})$. Equation (3) can be extended to a matrix that consists of all microphone probes,

$$\underbrace{\begin{bmatrix} e^{-ik^+x_1} & e^{ik^-x_1} \\ e^{-ik^+x_2} & e^{ik^-x_2} \\ \vdots & \vdots \\ e^{-ik^+x_m} & e^{ik^-x_m} \end{bmatrix}}_{\mathrm{A}} \cdot \underbrace{\begin{bmatrix} \hat{p}^+ \\ \hat{p}^- \end{bmatrix}}_{\mathrm{a}} = \underbrace{\begin{bmatrix} \hat{p}(x_1) \\ \hat{p}(x_2) \\ \vdots \\ \hat{p}(x_m) \end{bmatrix}}_{\mathrm{b}}. \tag{4}$$

The system can be solved by

$$a = A^+ b, \tag{5}$$

where A^+ is the Moore-Penrose pseudo-inverse (function available in Matlab) of A. The solution for a (the forward and backward traveling waves) is the best fit in the least square sense. The values of the Riemann invariants have to be calculated using an optimization technique that searches for the best fit of the input data. Since this method performs an average over several microphones, the flow noise is reduced (see Yang *et al.* [28]) and it overcomes the sensitivity to microphone spacing. In the current study three microphones have been considered and a distance of 0.15 m between the microphones has been applied. The distance from the vane to the nearest microphone is 0.15 m. The mics are positioned in the duct (can) section where the flow is homogeneous (not affected by the vanes).

3.7. Validity of planar wave assumption

To better understand the results shown in the plots, a calculation of the cut-off frequencies has been performed for both geometries under study. Below this cut-off frequency no propagation of higher modes is possible and the sound field consists of plane waves. In this situation, the recorded amplitudes of the analyzed microphones do not depend on the transversal location in the duct. The cut-off limit is dependent on duct radius, mean Mach number and speed of sound. The values of the cut-off limits have been calculated based on the cylindrical inlet section diameter for the 3D geometry and using the channel height for the 2D case. The cut-off frequency for the 3D case has been calculated as

$$\omega_c = \mu_{mn} \frac{c}{r} \sqrt{1 - M_x^2}, \tag{6}$$

where μ_{mn} is the n-th Eigenvalue of the Bessel function for the azimuthal mode m and r the radius of the circular section of the can. For 2D, the formula reads

$$\omega_c = \frac{c}{H} \sqrt{1 - M_x^2}, \tag{7}$$

with the channel height H.

For the 3D geometry the first higher radial and azimuthal modes can propagate above around 1300 Hz, at least in the circular section where an analytical estimation can be applied. As a consequence, results above this frequency might reveal deviations due to transversal waves,

pointing out the drop of accuracy shown by the method used. The results shown beyond the validity range (above $f = 1300\,\mathrm{Hz}$ up to $f = 2000\,\mathrm{Hz}$) are presented as information with the aim to perform in future further investigations in this higher frequency range with different post-processing methods. For the 2D case there are no higher modes propagating within the excitation frequency range used.

4. Analytical solutions

To assess the quality of the CFD results a comparison with analytical results is made where possible. Depending on the presence of flow, two types of analytical solutions are used for the comparison.

For the no flow cases, the 1D transfer matrix method is used. This approach is often used in 1D network models to analyze longitudinal combustor instabilities. For the simulations with flow a formulation proposed by Cumpsty and Marble [13] has been applied. In principle, both formulations could be applied with and without flow, but the divergence of the flow and acoustics propagation direction has to be considered first.

In the case of a quiescent fluid, the thermodynamic state on both sides of the vane passage is equal. The sound reflection is only influenced by the area blockage. The question to answer here is at which angle the sound waves leave the passage. In case of an undisturbed propagation direction the blockage can be approximated with a straight convergent-divergent nozzle with equal inlet and outlet cross-section on either end. In this case the transfer matrix method is easily applicable.

In case the sound waves follow the vane shape and deflect at least partially, the equivalent model for the transfer matrix would be a convergent nozzle, where the outlet cross-section is smaller than at the inlet.

For the case with a moving medium the flow acceleration and the corresponding drop in pressure and temperature have to be taken into account. Hence, for a correct reproduction of the thermodynamic conditions at the outlet the application of the 1D transfer matrix method is restricted to a convergent nozzle.

To have a correct flow, the geometry needs to be convergent. It is not possible to have correct (accelerated) flow with a convergent-divergent geometry model. The straight convergent-divergent scenario allows equal flow conditions which are not realistic in a real stator cascade. In the following, both analytical solutions are introduced.

4.1. Transfer matrix method

This method is valid for the assumption $\lambda \gg d$ where d represents the diameter of the geometry. To obtain the frequency dependent impedance and reflection coefficient of a duct with slowly varying cross-section the transfer matrix method can be used. In this method the geometry is sliced in a sequence of elements for which the transfer matrix is known. The transfer matrix relates the acoustic pressure and velocity at the inlet and outlet of each duct element. The relation reads [29]

$$\begin{bmatrix} p_1 \\ u_1 \end{bmatrix} = T \begin{bmatrix} p_2 \\ u_2 \end{bmatrix} \tag{8}$$

with

$$T = \mathrm{e}^{-\mathrm{i}Mk_cL} \begin{bmatrix} \cos(k_cL) & \mathrm{i}(\rho c/S)\sin(k_cL) \\ \mathrm{i}S/(\rho c)\sin(k_cL) & \cos(k_cL) \end{bmatrix}, \tag{9}$$

and L being the length, S the cross-section, and $k_c = k/(1-M^2)$ the wave number in each duct element. The response of the whole geometry is obtained by multiplying the transfer matrices of all duct elements,

$$T = T_1 \cdot T_2 \cdots T_n. \tag{10}$$

The termination is usually set to the free field impedance representing anechoic conditions or an infinite continuation of the duct. Finally the reflection coefficient can be calculated with

$$R = \frac{Z - Z_0}{Z + Z_0}, \tag{11}$$

where Z_0 is the local free field impedance and Z the impedance of the duct calculated from Equation (10).

4.2. Formulation of Cumpsty and Marble

An alternative analytical formulation to the transfer matrix method has been proposed by Cumpsty and Marble [13] to calculate the propagation of sound and entropy waves in a stator vane cascade. This model is based on the principle of the compact nozzle of Marble nd Candel [3] but considers a two-dimensional configuration. The solution has been applied more recently by Leyko *et al.* [12] and compared to CFD results. In this assumption (valid only in the limit of low frequencies) the characteristic wavelength λ of waves is longer as compared to the nozzle length L, $\lambda \gg L$. The paper of Cumpsty and Marble [13] presents the formula of the transmission coefficient $TC = w_2^+/w_1^+$ for a stator blade extended to flow without any references to the frequencies

$$TC = \frac{w_2^+}{w_1^+} = \frac{\mu_1}{\mu_2} \frac{1 + M_1\cos\theta_1 + \frac{w_1^-}{w_1^+}}{1 + \frac{M_2}{\cos\theta_2}}, \tag{12}$$

where $\mu = (1 + (\gamma - 1)M^2/2)^{-1}$, M_1 and M_2 are respectively the Mach numbers at inlet and outlet of the geometry, θ_1 and θ_2 the flow angles at inlet and outlet, w_2^+ reflected wave downstream and the reflection coefficient $R = w_1^-/w_1^+$ with w_1^- reflected wave upstream and w_1^+ incoming wave upstream side of the vane row

$$R = \frac{w_1^-}{w_1^+} = -\frac{1 + \frac{1}{M_1\cos\theta_1} - \frac{\mu_1}{\mu_2}\frac{(1+M_1\cos\theta_1)(M_2\cos\theta_2+1)}{M_2(\cos\theta_2+M_2)}}{1 - \frac{1}{M_1\cos\theta_1} - \frac{\mu_1}{\mu_2}\frac{(1-M_1\cos\theta_1)(M_2\cos\theta_2+1)}{M_2(\cos\theta_2+M_2)}}. \tag{13}$$

The formulation of the transmission coefficient proposed in Equation (13) has been applied to the 2D single vane

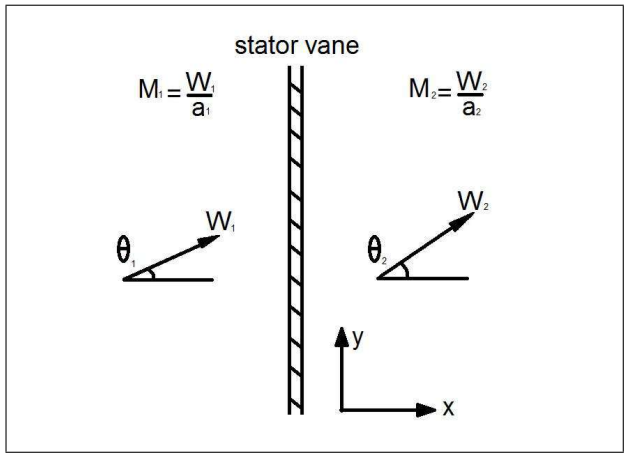

Figure 4. Stator vane model rapresentation according to Cumpsty and Marble [13].

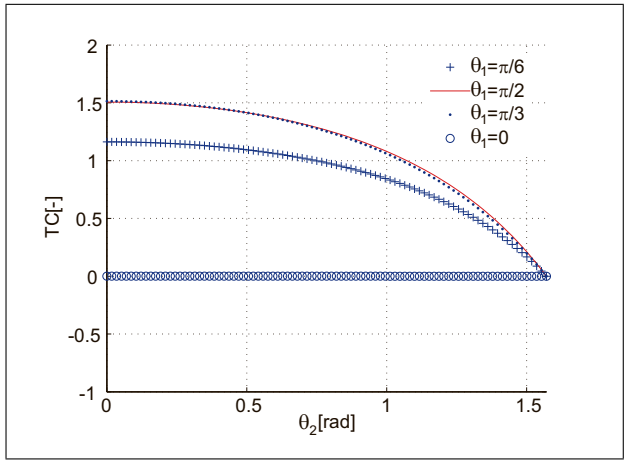

Figure 5. Analytical formula in Equation (12) applied to 2D single vane.

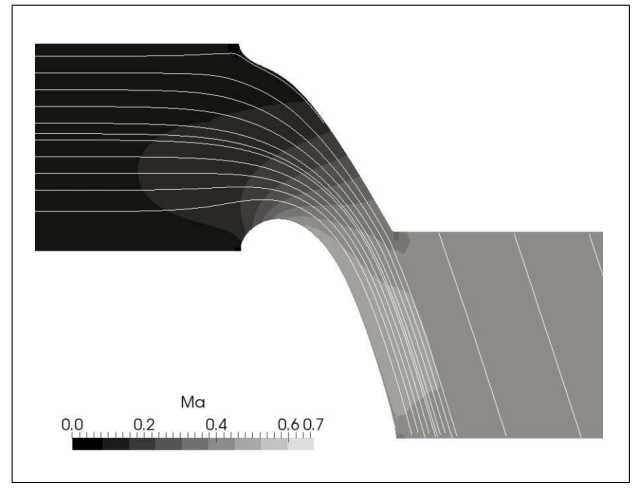

Figure 6. The distribution of the Mach number in the stator passage is presented for the 2D single vane case.

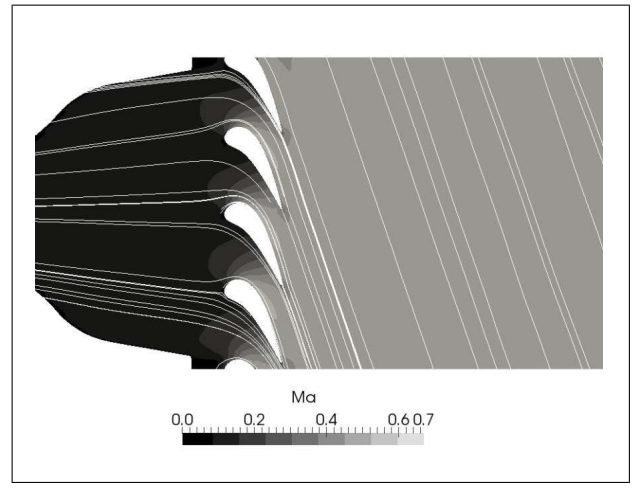

Figure 7. The distribution of the Mach number in the stator passage is presented for a slice cut of the 3D geometry.

and 3D geometries (see Figure 5) showing the same trend presented in [12] in Figure 4b. In Figure 4 the relative velocity vectors W_1 and W_2 and the flow angles θ_1 and θ_2 on both sides of the vane row are shown as clarification.

The Figure 4b shown in [12] compares the results obtained from the 2D model configuration made by Cumpsty and Marble [13] with the 1D compact nozzle model of Marble and Candel [3]. The ratio of the acoustic responses at the outlet of the vane row w_2^+ and the acoustic one at the inlet w_1^+ have been plotted for different inlet and outlet flow angles θ_1 and θ_2. The 2D and 1D models show different results for several flow deviations, but for $\theta_1 = \theta_2$ both theories coincide. Figure 5 in the current paper validates the results obtained for the current 2D geometry studied together with the outcomes presented in Leyko *et al.* [12] in Figure 4b for the 2D model. In the current cases values of $M_1 = 0.15$, $M_2 = 0.7$, $\theta_1 = 0\,\text{rad}$ and $\theta_2 = 1.36\,\text{rad}$ have been considered, but Figure 5 shows the same range of flow angles θ_1 and θ_2 used also in Leyko *et al.* [12] in Figure 4b in order to represent the same trend of Leyko *et al.* [12] for the 2D model. The amplitude of TC is decreasing monotonically with θ from about 1.2 at $\theta_2 = 0$ to 0 at $\theta_2 = 1.5\,\text{rad}$.

5. Results

The numerical results obtained for the 2D and 3D configurations shown in the previous sections will be compared below since their flow structures are equivalent. In this section a detailed study has been performed pointing out the acoustical behavior and comparisons for both geometries.

5.1. Flow Field

At first, the flow obtained by the numerical flow simulation has been presented for both configurations. Figure 6 and Figure 7 depict the Mach behavior along the 2D and 3D geometries.

For the 3D engine, the Mach trend has been shown along a cut plane containing the vanes. In the same plots also streamlines representing the deviation of the flow

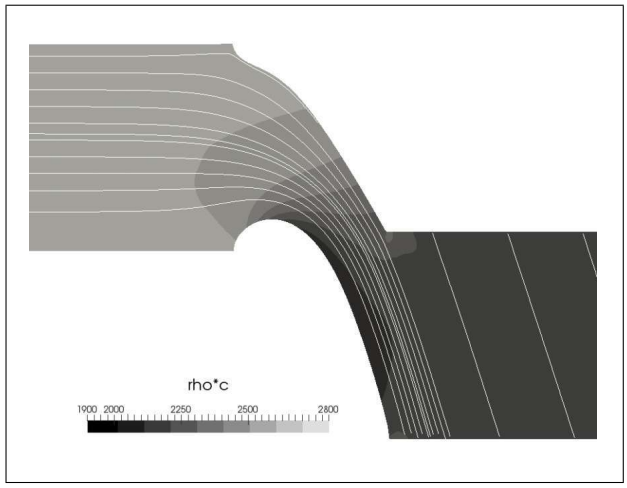

Figure 8. The distribution of the wave impedance in the stator passage is shown for the 2D single vane case.

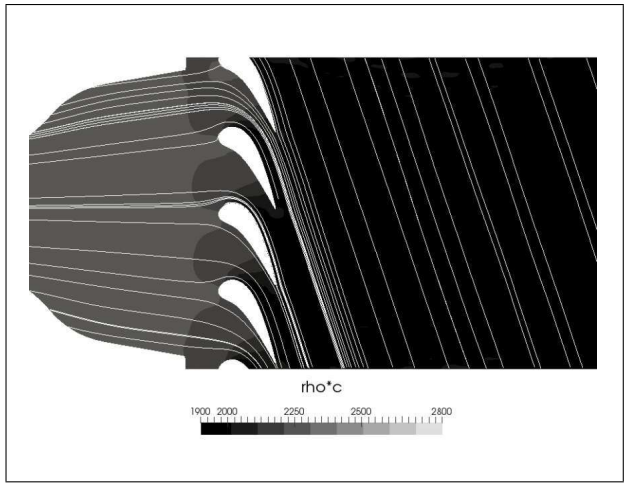

Figure 9. The distribution of the wave impedance in the stator passage is shown for a slice cut of the 3D geometry.

have been included. In Figure 6 and Figure 7 it can be observed how the flow is deflected by the vanes. Due to the deflection the flow is accelerated, leading to an increase of the Mach number to about 0.6.

Figure 8 and Figure 9 present the plane wave impedance $Z_0 = \rho * c$ obtained along the configurations.

This quantity has been chosen to represent the thermodynamic state change caused by the acceleration of the flow in the stator. For the chosen Mach number, a decrease of Z_0 by a factor of 1.5 can be observed for both geometries.

5.2. Reflection Coefficient

The reflection coefficient obtained from the numerical simulations is analyzed for all configurations. The results analyzed with the multi-microphone method have been compared and shown for the 2D and 3D configurations.

5.2.1. Non-reflective termination

The non-reflecting boundary conditions applied have been verified at the outlet. In the ideal case, the result is not influenced by unphysical waves reflected by the NRBC. The ideal reflection factor is hence $R = 0$. R_{out} represents the reflection coefficient measured at the outlet in order to validate the NRBC in the cases of no flow (2D geometry) and flow (for 2D and 3D configurations) shown in Figure 10a and Figure 10b. R_{out} shows a smoother behavior around zero with average reflection coefficient of 0.1 for intermediate and high frequencies for the 2D configuration, but it shows reflection for low frequencies. In case of the 3D configuration with flow the reflection at the outlet reached higher average values around $R_{\text{out}} = 0.15$.

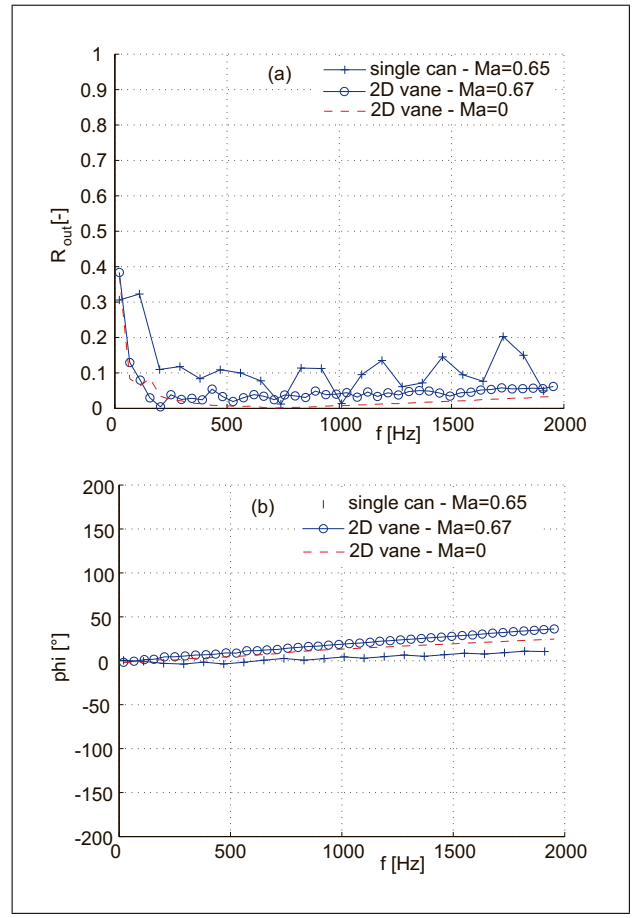

Figure 10. 2D versus 3D configurations. (a) Reflection coefficient spectrum at outlet, (b) Reflection coefficient phase at outlet.

For low frequencies all geometries present reflection that can be attributed to imperfect behavior of the CFD solutions. The reflection factors grow to significant values for low frequencies and might result in inaccurate data in this range. The growth is attributed to the boundary condition formulation where a relaxation factor is used to set a trade-off between the non-reflectiveness and the controllability of mean values.

The non-reflecting boundary condition formulation employed uses a relaxation term to ensure that the temporal average at the boundary condition is close to the target value. For practical simulations the boundary condition time scale should be as small as possible to avoid large deviations of the boundary conditions from the prescribed mean value. For small time scales, however, the

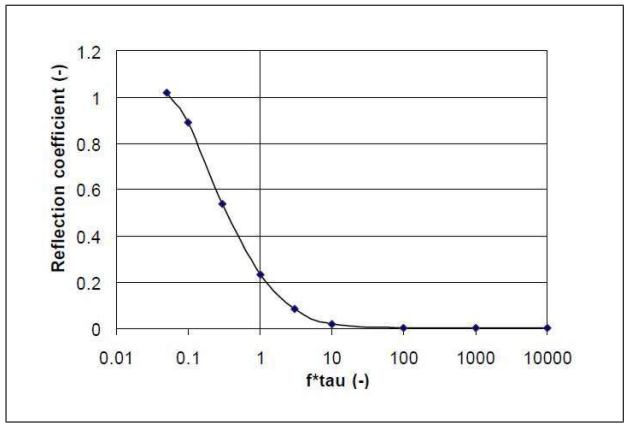

Figure 11. Impact of the boundary condition time scale on the reflection coefficient.

boundary conditions become fully reflective. Thus, a compromise needs to be identified. In Figure 11 the measured reflection coefficient of the outlet boundary condition for a range of relaxation time scales is shown.

The relaxation time scale is normalized with the oscillation frequency. To achieve a low reflection coefficient in practical simulations the product of the lowest frequency of interest and the relaxation time scale should be ≈10. In the current paper, the value of 10 is reached for a time scale of 0.01 and for the frequency of interest of 1000 Hz. For the current lowest frequency of 20 Hz with the same time scale of 0.01 we reach a value of 0.2 that corresponds to higher values of reflection coefficient. The range of frequencies is too wide in the current study and this value of time scale has been chosen as the best compromise but the accuracy is reduced for lower frequencies.

5.2.2. Reflection at the stator passage

The results showing the reflection coefficient R behavior have been calculated for the 2D and 3D geometries in the point located at the leading edge of the vane. The choice of the reference point has no influence on the reflection coefficient magnitude, but influences the phase.

5.2.3. Reflection without flow

The computed 2D vane Reflection Coefficient is presented in Figure 12a (magnitude) and Figure 12b (phase) and compared with the analytical formulation in Equation (11). For the no flow case, the numerical simulations have been compared with the analytical transfer matrix method results described above. The vane passage cross-sections have been approximated along the center stream line mapping the vane stage to a 1D geometry similar to a convergent-divergent nozzle configuration. The 3D case results without flow have been not taken into consideration in the current analysis because the speed of propagation is the same in all directions since it is not forced by the flow field into the flow direction. For this reason the multi-microphone method is not appropriate to analyze this case. The 2D geometry without flow shows good results anyway due to the fact that the configuration is simpler compared to the 3D case.

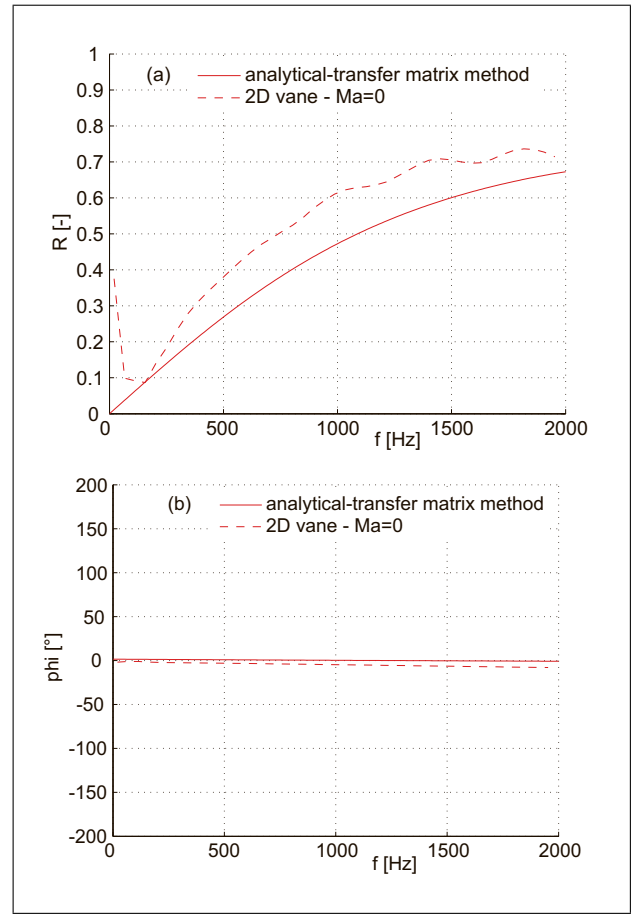

Figure 12. Reflection coefficient phase for 2D and 3D cases compared to analytical formulation. Reflection coefficient (a) magnitude and (b) phase for the 2D case compared to analytical formulation in Equation (11): no flow.

For the R analyzed before the vane section, the numerical curve representing the 2D geometry follows the analytical formula presenting the same trend. The reflection is higher in the 2D numerical results as compared to the analytical method. The behavior shown by R reaches a maximum value around $R = 0.7$ maintaining then a flatter trend starting from $f = 1500$ Hz. The change of the behavior at $f = 500$ Hz might be attributed to low quality of the CFD solutions in the low frequency range.

5.2.4. Reflection with flow

For situations with flow (see Figure 13) the numerical results related to the reflection coefficient magnitude for all configurations have been compared with the low frequency approximation by Cumpsty and Marble [13] in Equation (13).

Since both configurations present the same flow angle and Mach conditions at inlet and outlet, the same results obtained from the analytical formulation have been taken into account as comparison with the numerical simulations. In case of flow the curves representing the numerics are steeper with higher values of R between $R = 0.6$ and $R = 0.8$ for the increased Mach number.

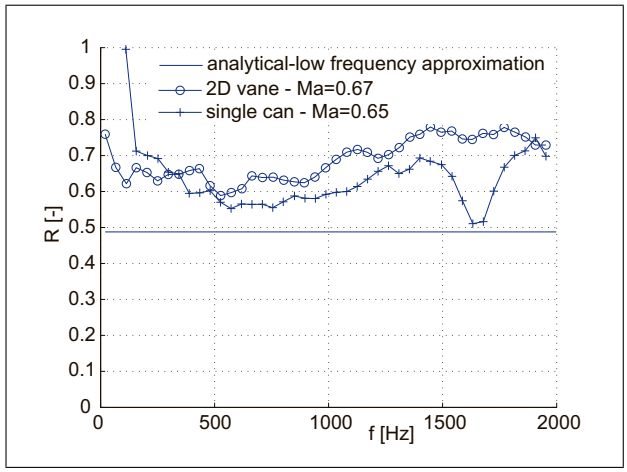

Figure 13. Reflection coefficient magnitude for 2D and 3D cases compared to analytical formulation in Cumpsty and Marble [13] in Equation (13): flow.

It is expected that the geometry effects could be responsible. The analytical formulation in Cumpsty and Marble [13] is not assuming the change in density over the vanes but in the current study a reduction of density and temperature because of acceleration could cause this effect. In the 3D case short physical times have been simulated and the results have been shown as rough comparisons. Probably the short times caused the cpsd (cross power spectral density) function in the microphone method to use inaccurate windowing and resolution values. The 3D case is a new topic and it has been taken into account in order to give a first comparison with the performances of the 2D cases.

Figure 14a and 14b show the flow study performed for the 2D single vane. Several simulations have been run starting with a case without flow arriving to Mach number $M \approx 0.8$. As shown before for no flow, the reflection curve shows a trend with values that are increasing from $R = 0$ to $R = 0.7$. In case of flow in Figure 14a the curve with $M = 0.67$ is flatter than the curve for $M = 0$ maintaining constant at higher values of R between $R = 0.6$ and $R = 0.8$. For higher Mach number of $M = 0.81$ the curve shows higher values of reflection coefficient compared to the case with $M = 0.67$ in the frequency range up to $f = 1000$ Hz. Above $f = 1000$ Hz the numerical results are misleading due to the fact that the post-processing method used becomes less accurate in this higher frequency range.

Figure 15a and Figure 15b present the comparisons between the 2D geometry with no flow and with $M = 0.67$ and the 3D real engine for $M = 0.65$. The two curves with high Mach show an accurate agreement in the frequency range up to $f = 1500$ Hz with a similar trend of reflection coefficient with overall constant values around $R = 0.7$.

5.3. Analysis of the sound propagation direction

An important aspect of the sound transmission though an airfoil passage is the change of the sound propagation angle. While the deflection of the mean flow is obvious, the

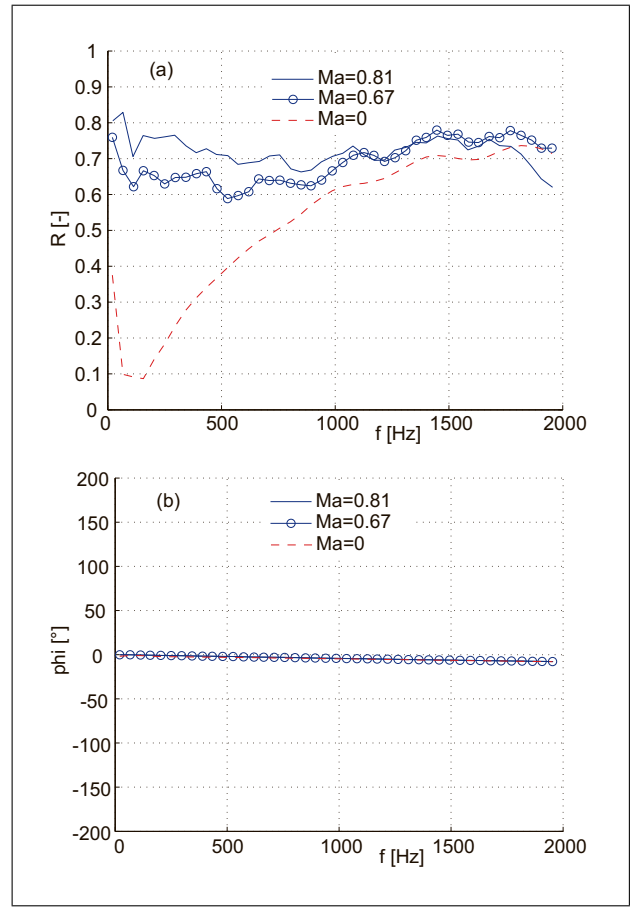

Figure 14. 2D single vane flow study - Reflection coefficient magnitude (a) and phase (b).

behavior of the acoustic perturbations behind the passage is not. Based on the detailed numerical data available, an analysis of the radiation direction has been performed. The procedure is described below. For reason of geometrical simplicity the 2D case has been used for the investigation. The unsteady pressure signal has been sampled along a curve spanning from the inlet section to the outlet of the computational domain. The line location is plotted in Figure 16 and the data plotted over space and time are depicted in Figure 17. The plot reveals lines of constant positive and negative inclination representing downstream and upstream propagation of sound. Some steeper lines attached to the vane indicate convective propagation of turbulent structures over a short distance.

To gain insight into the sound propagation angle behind the vane, the propagation delay between two points on the lines (indicated by the two dashed lines in Figure 17 at $x = 0.45$ m and $x = 1$ m) has been calculated using the cross-correlation of the temporal signals at these two locations.

The available data from the CFD results, namely the flow velocity components, speed of sound (from temperature) and the calculated propagation delay can be combined graphically as shown in Figure 18.

The average convective speed vector $[U_x, U_y]$ is the origin of the circle with a radius equal to the speed of sound c in the section downstream the vane. The effective axial

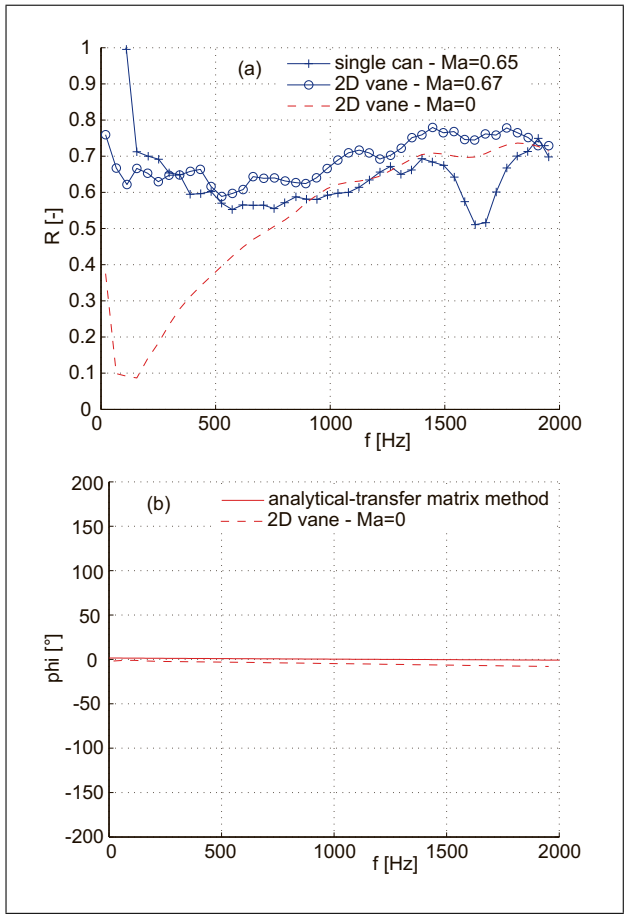

Figure 15. 2D versus 3D configurations - Reflection coefficient magnitude (a) and phase (b).

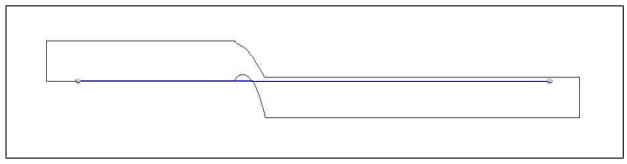

Figure 16. Axial distance taken into account for the analysis of the 2D vane.

propagation velocity is derived from the cross-correlation delay and the line distance. It is indicated by the vertical dashed line in the plot at about 1000 m/s. Knowing that sound propagates axially with $U_x + c$, the propagation angle can be found by finding the intersection of the vertical line and the circle. The intersection in the particular case is two-fold and at about ±7°. Due to the fact that the propagation is at an angle relative to the microphone distribution, a mismatch in propagation speed could be provoked. However, the difference is very small considering the 7° angle and the major component of the propagation velocity is in longitudinal direction. In this case the use of the two and multi-microphone methods is still justified. Both solutions are mathematically valid, but the solution closer to the flow direction appears more physical. In conclusion, the acoustic propagation angle changes only slightly compared to the mean flow when the sound passes the stator stage.

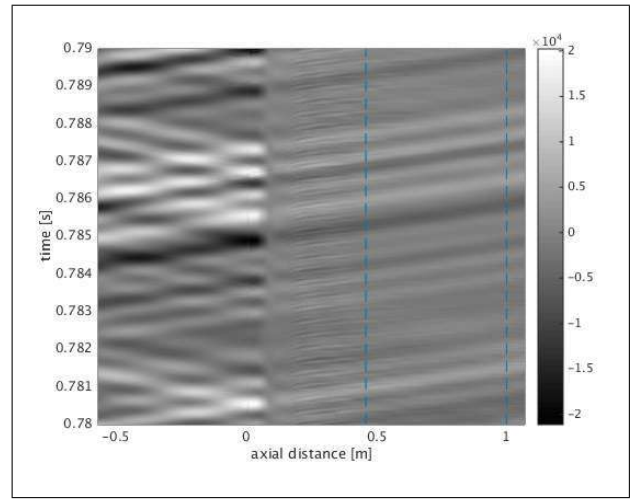

Figure 17. Time evolution of the pressure signal analyzed.

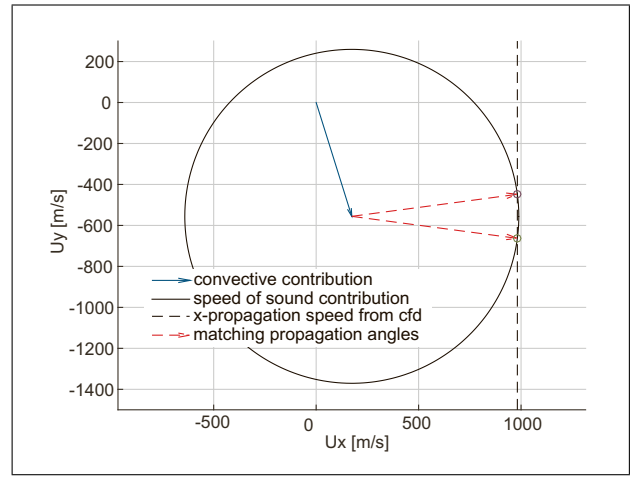

Figure 18. 2D vane sound propagation angle analysis.

6. Conclusion

Two models of different complexity have been analyzed in this paper and numerical results have been compared with analytical formulae. The CFD open source code OpenFOAM has been used for the numerics. The forced response approach has been applied provoking a wave excitation at the inlet of each geometry. For both configurations a frequency range of $f = 20 - 2000$ Hz has been considered. Sampling data at probes have been pointed out from the simulations and used in the post-processing analysis. A detailed study of the reflection coefficient R behavior before the vanes has been performed for the 2D and 3D geometries. The reflection coefficient has been analyzed also at the outlet in order to validate the NRBC. The results obtained present an average reflection of 0.1 that does not affect significantly the simulations. For low frequencies all geometries present reflection that can be also in these cases attributed to low quality of the CFD solutions at low frequency. The 2D geometry and the 3D real engine present equivalent flow structures giving the possibility to make an accurate comparison. In case of no flow the 2D config-

uration has been compared with the analytical formulation of the 1D transfer matrix method. For comparison with the numerical results, a convergent-divergent nozzle has been chosen as equivalent model for the 1D transfer matrix. This approximation has been proved in this work pointing out that the sound wave propagation follows quite straight the vane shape. The numerical results follow the analytical trend overall in an accurate way. In case of flow the behavior of the analytical approximation shown in Cumpsty and Marble [13] has been evaluated and compared with the 2D and 3D numerical results. It needs to be taken into account that the analytical formula does not consider the effects of the turbulence contrary to the numerics. This can explain the overall higher values of reflection coefficient shown in the numerics compared to the analytical approximation. The numerical results follow the analytical trend with reasonable agreement. The sound propagation angle behind the vane has been also analyzed. For higher Mach number of about 0.7 a small deviation of about 7° from the mean flow direction has been revealed. The numerical results shown for both 2D and 3D geometries pointed out overall a good agreement between the two configurations as expected.

Acknowledgement

The authors would like to thank Niclas Hanraths that developed the code for the multi microphone methods.

Funding

The numerical research presented in this paper has received funding from the European Community's Seventh Framework Programme (FP7, 2007-2013), PEOPLE programme, under the grant agreement No FP7-290042(COPAGT project).

References

[1] S. Candel: Analytical Studies of Some Acoustic Problems of Jet Engines. PhD Thesis, California Institute of Technology, Pasadena, California, 1972.

[2] F. Marble: Acoustic disturbance from gas nonuniformities through a nozzle. Proc. Interagency Symp. Univ. Res. Transp Noise, Stanford University, 1973, 3.

[3] F. Marble, S. Candel: Acoustic disturbances from gas nonuniformities convected through a nozzle. Journal of Sound and Vibration **55**(2) (1977) 225–243.

[4] M. Leyko, F. Nicoud, T. Poinsot: Comparison of direct and indirect combustion noise mechanisms in a model combustor. AIAA Journal **47** (November 11 2009) 2709–2716.

[5] L. Crocco: Supercritical gaseous discharge with high frequency oscillations. Aerotechnica **33**(1) (1953) 46–53.

[6] H. S. Tsien: The transfer functions of rocket nozzles. Journal American Rocket Society **22** (May–June 3 1952) 139–143.

[7] F. Bake, N. Kings, A. Fischer, I. Rohle: Experimental investigation of the entropy noise mechanism in aero–engines. International Journal of Aeroacoustics **8**(1) (2009) 125–142.

[8] N. Lamarque, T. Poinsot: Boundary Conditions for Acoustic Eigenmode Computations in Gas Turbine Combustion Chambers. AIAA Journal **46**(9) (2008).

[9] B. Mühlbauer, B. Noll, M. Aigner: Numerical investigation of the fundamental mechanism for entropy noise generation in aero–engines. Acta Acustica united with Acustica **95** (2009) 470–478.

[10] M. Leyko, F. Nicoud, S. Moreau, T. Poinsot. Numerical and analytical investigation of the indirect combustion noise in a nozzle. Comptes Rendus Mecanique **337**(6–7) (2009) 415–425.

[11] I. Duran, S. Moreau, T. Poinsot. Analytical and numerical study of direct and indirect combustion noise through a subsonic nozzle. AIAA Journal **51**(1) (2013) 42–52.

[12] M. Leyko, I. Duran, S. Moreau, F. Nicoud, T. Poinsot: Simulation and modelling of the waves transmission and generation in a stator blade row in a combustion–noise framework. Journal of Sound and Vibration **333** (2014) 6090–6106.

[13] N. Cumpsty, F. Marble: The interaction of entropy fluctuations with turbine blade rows; a mechanism of turbojet engine noise. Proceedings of the Royal Society of London **357** (1977) 323–344.

[14] R. S. Muir: The application of a semi–actuator disk model to sound transmission calculations in turbomachinery. Part I.: the single blade row. Journal of Sound and Vibration **54** (October 3 1977) 393–408.

[15] R. S. Muir: The application of a semi–actuator disk model to sound transmission calculations in turbomachinery. Part II.: multiple blade rows. Journal of Sound and Vibration **55** (October 3 1977) 335–349.

[16] S. Kaji, T. Okazaki: Propagation of sound waves through a blade row: I. Analysis based on the semi–actuator disk theory. Journal of Sound and Vibration **11** (March 3 1970) 339–353.

[17] S. Kaji, T. Okazaki: Propagation of sound waves through a blade row: II. Analysis based on the acceleration potential method. Journal of Sound and Vibration **11** (March 3 1970) 355–375.

[18] H. Posson, S. Moreau, H. Beriot, Y.B. de l'Epine, C. Schram: Prediction of sound transmission through an annular cascade using an analytical cascade response function. The 16th AIAA/CEAS Aeroacoustics Conference and Exhibit Stockholm, Sweden–AIAA Paper 2010–4030, 2010.

[19] H. Posson, M. Roger: Parametric study of gust scattering and sound transmission through a blade row. The 13th AIAA/CEAS Aeroacoustics Conference and Exhibit Rome, Italy, AIAA Paper 2007–3690, 2007.

[20] L. Selle, F. Nicoud, T. Poinsot: Actual Impedance of Nonreflecting Boundary Conditions: Implications for Computation of Resonators. AIAA Journal **42**(5) (2004).

[21] S. Jaensch, C. Sovardi, W. Polifke: On the robust, flexible and consistent implementation of time domain impedance boundary conditions for compressible flow simulations. Journal of Computational Physics **314** (2016) 145–159.

[22] W. Polifke, C. Wall: Non–reflecting boundary conditions for acoustic transfer matrix estimation for LES. Proceedings of the Summer Program, 2002, 345–356.

[23] A. Widenhorn, B. Noll, M. Aigner: Accurate boundary conditions for the numerical simulation of thermoacoustic phenomena in gas–turbine combustion chambers. Proceedings of ASME Turbo Expo GT2006–90441, Barcelona, Spain, 2006.

[24] B. B. H. Schuermans: Modeling and control of Thermoacoustic instabilities. PhD Thesis, École Polytechnique Fédérale de Lausanne, 2003.

[25] W. Polifke, C. O. Paschereit, T. Sattelmayer: A universally applicable stability criterion for complex thermoacoustic systems. VDI–Berichte (1997) 455–460.

[26] C. O. Paschereit, W. Polifke: Investigation of thermoacoustic characteristic of lean premix gas turbine burner. ASME 98–GT–0582, ASME Turbo Expo 1998 Stockholm, June 2–5, 1998.

[27] C. O. Paschereit, B. B. H. Schuermans, W. Polifke, O. Mattson: Measurements of transfer matrices and source terms of premixed flames. Journal of Engineering for Gas Turbines and Power **124**(2) (2002) 239–247.

[28] F. Yang, Z. Guo, X. Fu: Computation of Acoustic TRansfer Matrices of Swirl Burner with Finite Element and Acoustic Network Method. Journal of Low Frequency Noise, Vibration and Active Control **34** (2015) 169–184.

[29] F. P. Mechel: Formulas of Acoustics. Springer, 2008.